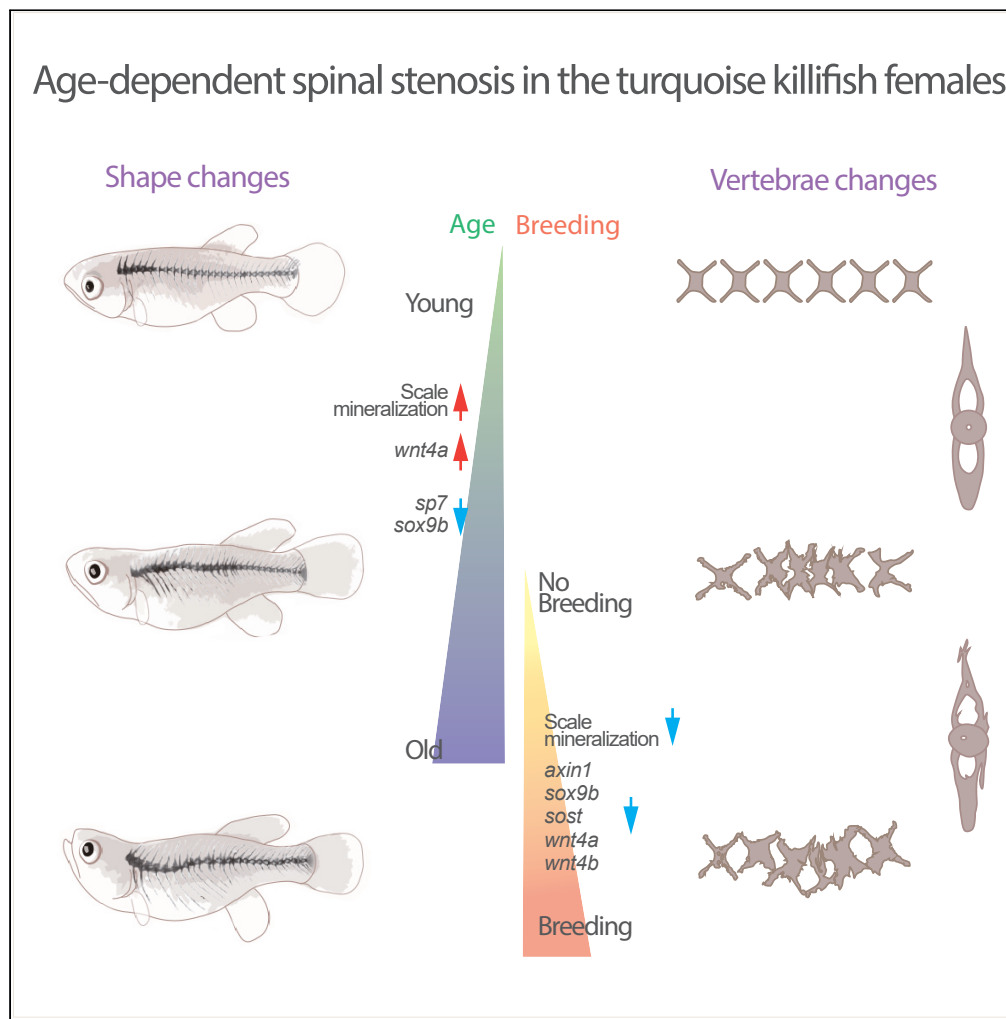


Article

Age-associated spinal stenosis in the turquoise killifish



Su-Hyeon Cho,
Seongsin Lee, Jae-Il Park, ..., Nayoung Gwak, Kil-Nam Kim, Yumi Kim

knkim@kbsi.re.kr (K.-N.K.)
yumikim@unist.ac.kr (Y.K.)

Highlights

Aged killifish showed shape changes and vertebrae collapse, worsened by spawning

Micro-CT showed the structural deformation of vertebrae by aging and spawning

Vertebrae deformation can be tracked by scale mineralization and gene expression

The turquoise killifish may offer a model for studying human spinal stenosis



Article

Age-associated spinal stenosis in the turquoise killifish

Su-Hyeon Cho,^{1,2,9} Seongsin Lee,^{3,8,9} Jae-Il Park,^{4,9} Yoon La Yang,⁴ Song-Rae Kim,^{1,2} Juhee Ahn,² Hoibin Jeong,^{1,7} Hye-Yeon Jung,⁴ Nayoung Gwak,^{3,8} Kil-Nam Kim,^{1,5,*} and Yumi Kim^{3,6,8,10,*}

SUMMARY

Aging triggers spinal degeneration, including common spinal stenosis, which causes back and leg pain in older individuals, significantly impacting their quality of life. Here, we explored aging traits in turquoise killifish spines, potentially offering a model for age-linked spinal stenosis in humans. Aged turquoise killifish exhibited body shape deformation and increased vertebral collapse, which was further accelerated by spawning. High-resolution CT scans revealed suppressed cortical bone thickness and hemal arch area in vertebrae due to spawning, and osteophyte formation was observed in both aged and breeding fish populations. Scale mineralization mirrored these changes, increasing with age but being suppressed by spawning. The expression of *sp7*, *sox9b*, *axin1*, and *wnt4a/b* genes can be utilized to monitor age- and reproduction-dependent spine deformation. This study demonstrates that turquoise killifish and humans share certain phenotypes of age-related vertebral abnormalities, suggesting that turquoise killifish could serve as a potential model for studying human spinal stenosis.

INTRODUCTION

Bones have important mechanical, metabolic, and synthetic functions, protect internal organs, strengthen locomotion and load-bearing, provide a cavity for marrow, and function in the regulation of calcium homeostasis.^{1–3} The spine is located in the center of the body, facilitates body movement, and balances body weight distribution during movement or static posture.⁴ These functions decrease considerably with age, often resulting in chronic pain. Age-related degenerative changes frequently occur in the neck and lower back, which are referred to as cervical stenosis and lumbar stenosis, respectively. Spinal stenosis can be diagnosed by MRI or computed tomography (CT). Symptoms of spinal stenosis vary depending on its location and include neuropathy, such as numbness or tingling in the hand, arm, foot, and/or leg, weakness of the hands, arms, feet, and/or legs, pain in the neck or back, and problems with walking and balance.⁵ Treatments for spinal stenosis have mainly focused on relieving symptoms, including surgical decompression and pharmacological treatments. However, the development of preventive measures or functional cures for spinal stenosis will require elucidating its underlying molecular mechanisms.

Spinal stenosis is mainly caused by osteoarthritis. In addition to stenosis, osteoarthritis also leads to abnormal mineralization, such as sclerosis, and cyst and osteophyte formation.⁶ Mineral homeostasis of the bone is achieved by the orchestrated actions of hormones such as vitamin D (cholecalciferol), parathyroid hormone, estrogen, and calcitonin, and involves various cell types such as osteoblasts, bone lining cells, osteocytes, and osteoclasts.⁷ Wingless (*Wnt*), receptor activator of nuclear factor kappa-B (NF- κ B) (RANK), receptor activator of NF- κ B ligand (RANKL), and osteoprotegerin (OPG) pathways regulate bone remodeling in subchondral bone. Osteoclasts are large multinucleated cells that differentiate upon exposure to RANKL, which binds to the RANK receptor on the osteoclast surface.^{8–10} Osteoblasts have roles in bone formation and are localized to the bone surface. Mesenchymal stem cells differentiate into osteoblasts under the control of bone morphogenic protein and *Wnt* pathways.^{11,12} *Runt-related transcription factor 2 (RUNX2)* is a key player in osteoblast differentiation and induces the expression of osteoblast-related genes including *type-I collagen*, *bone sialoprotein*, and *osteocalcin*.¹³ Osteocytes derived from osteoblasts comprise 90%–95% of bone cells and can survive for a long time within lacunae. Osteocytes are mechano-sensitive cells. However, it is still unclear how dysregulation of these various factors and cells contributes to spinal stenosis.

¹Chuncheon Center, Korea Basic Science Institute, Chuncheon 24341, Republic of Korea

²Department of Medical Biomaterials Engineering, College of Biomedical Sciences, Kangwon National University, Chuncheon 24341, Republic of Korea

³Center for Plant Aging Research, Institute for Basic Science, Daegu 42988, Republic of Korea

⁴Animal Facility of Aging Science, Korea Basic Science Institute, Gwangju 61751, Republic of Korea

⁵Department of Bio-analysis Science, University of Science & Technology, Daejeon 34113, Republic of Korea

⁶Center for Genome Integrity, Institute for Basic Science, Ulsan 44919, Republic of Korea

⁷Seoul Center, Korea Basic Science Institute, Seoul 02841, Republic of Korea

⁸Present address: Korean Genomics Center, Biomedical Engineering, UNIST, Ulsan 44919, Republic of Korea

⁹These authors contributed equally

¹⁰Lead contact

*Correspondence: knkim@kbsi.re.kr (K.-N.K.), yumikim@unist.ac.kr (Y.K.)

<https://doi.org/10.1016/j.isci.2023.107877>



Teleost fish have been used as animal models because their molecular, cellular, and physiological aging phenotypes show remarkable similarities with those of other vertebrates, including humans.^{14–16} X-ray CT scans and alizarin red S staining analysis have been used to study bone formation in teleost fish, such as medaka, zebrafish, and juvenile fish.^{17–21} Aging has been previously studied in zebrafish using CT, as zebrafish are an excellent animal model for studying diseases and development in vertebrate.^{17,18,20,21} However, zebrafish have an average maximum lifespan of 3–5 years under laboratory conditions,¹⁹ which restricts the study of natural aging in these fish. The African turquoise killifish has emerged as a promising model of aging due to its short lifespan, which ranges from 9 to 26 weeks, depending on its ecotypes.²² Although the turquoise killifish has a short lifespan, they exhibit conserved aging phenotypes, including body color loss, spinal curvature, emaciation, age-dependent gene expression, neurodegeneration, and increased susceptibility to cancer.^{16,23,24} Age-dependent spine curvature is frequently observed in aged turquoise killifish and especially in breeding females, but its characteristics and the possibility that killifish could be used as a model to study age-related bone diseases have not been investigated.

In this study, we quantified age- and breeding-dependent body shape and spine structures to identify the skeletal alterations that occur during aging in female turquoise killifish. We found that the head and tail tended to curve upward during aging and breeding, using bone staining with alizarin red S and high-resolution micro-CT. Spinal curvature and stenosis were clearly observed upon aging and breeding, which were quantitatively analyzed by measuring bone volume (BV), bone volume fraction (BV/TV), bone mineral density (BMD), and cortical bone properties. Gene expression analysis identified genes whose expression was associated with aging and spawning, including those belonging to molecular pathways of bone homeostasis. Gene expression marker screening allowed the identification of age, breeding, and age-bio-markers of bone aging. The results strongly suggest that the turquoise killifish has the potential as a model organism for the study of degenerative bone diseases associated with natural senescence and breeding. Deciphering the detailed mechanisms of age-dependent spinal stenosis in turquoise killifish could lead to the discovery of new drugs for the treatment of human bone diseases.

RESULTS

The turquoise killifish spine hunches with aging and during breeding

Body lengths were firstly measured in 5-, 9-, and 14-week-old female fish to check age-dependent growth and to test for a possible effect of breeding on growth (Figure S1). After hatching, body length significantly increased between 5 and 9 weeks of age and showed an increasing trend without statistical significance between 9 and 14 weeks of age. However, breeding suppressed the growth of female fish (Figure S1). Interestingly, each experimental group of female fish showed different degrees of body curvature (Figure 1A). We employed geometric morphometric analysis to quantify body shape during aging and with and without breeding. We set 58 landmarks along the body shape of fish from each experimental group and analyzed the changes in body shape regardless of body size (Figure S2). In each experimental group, shape changes relative to the average body shape were expressed in terms of direction and length. Nine-week-old fish with breeding had a body shape that was closest to that of the average body shape. In 5- and 9-week-old fish without breeding, the head and tail were oriented downward compared to those of the average body shape. Conversely, in 14-week-old fish without breeding, the head and tail were oriented upward compared to those of the average body shape. In 14-week-old female fish with breeding, the orientation of the head upward and the belly downward were more severe than in 14-week-old fish without breeding (Figure 1B). These differences were visualized again using wireframes, which confirmed that fish aging and breeding are associated with distinct body shapes (Figure 1C). Additionally, we performed a principal component analysis to identify the critical components of body shape. The first principal component (PC1) explained over 60% of the total variance (Figure 1D; Figure S3). When we plotted individual fish scores based on PC1 and PC2, confidence ellipses for mean values for 14-week-old female fish after breeding were clearly separated from those for 5- and 9-week-old fish without breeding (Figure 1E). Spinal curvature leads to upward positions of the head and tail and a downward position of the belly, and the area of the spine closest to the head is weakened during aging and breeding.

Whole bone architectures of female fish, with respect to aging and breeding status, were further examined using alizarin red S staining after tissue clearing (Figure 2; Figure S4). The turquoise killifish spine can be divided into Weberian, precaudal (abdominal), caudal, and caudal fin vertebrae, totaling 29 vertebrae (Figure S4). As expected, the spine was severely bent in female fish during breeding. Additionally, turquoise killifish exhibited increasing vertebral collapse with aging and breeding (Figure 2, purple insets). Abnormal vertebral stacking was rarely observed in 5-week-old female fish but was severe in aged fish and those with breeding. Fish with breeding showed early development of spinal abnormalities at 9 weeks after hatching (Figure 2). These results suggest that the deformation of vertebrae near the head involves both spinal curvature and collapse in aged and reproducing females.

Spawning inhibits natural bone growth of the female turquoise killifish

A morphometric analysis by micro-CT was performed to examine bone growth with respect to age and breeding status based on various parameters, such as BV/TV, BMD, BV, bone surface (BS), and average bone thickness (B.Th) in whole fish (Figure 3A, Video S1). The BV/TV ratio was significantly higher in 9- and 14-week-old fish than in 5-week-old fish. Additionally, the BS area and B.Th were significantly higher in 9- and 14-week-old fish than in 5-week-old fish. Similar to bone growth, the BMD of whole bone increased with age, irrespective of breeding status (Figure 3B). However, in 9- and 14-week-old fish with breeding, bone growth was significantly suppressed as evidenced by the lower BV/TV ratio, BV, BS, and B.Th values relative to those of the control groups.

Spine curvature and vertebral collapse were observed between the precaudal and caudal vertebrae in the Weberian vertebrae; thus, we focused on 1) vertebrae 1–5 (VOI1) and 2) vertebrae 14–18 (VOI2) (Figure 4A). BV/TV ratios in both VOI1 and VOI2 were significantly higher in 9- and 14-week-old fish than in 5-week-old fish. BMD in either VOI1 or VOI2 was not significantly different irrespective of the fish group.

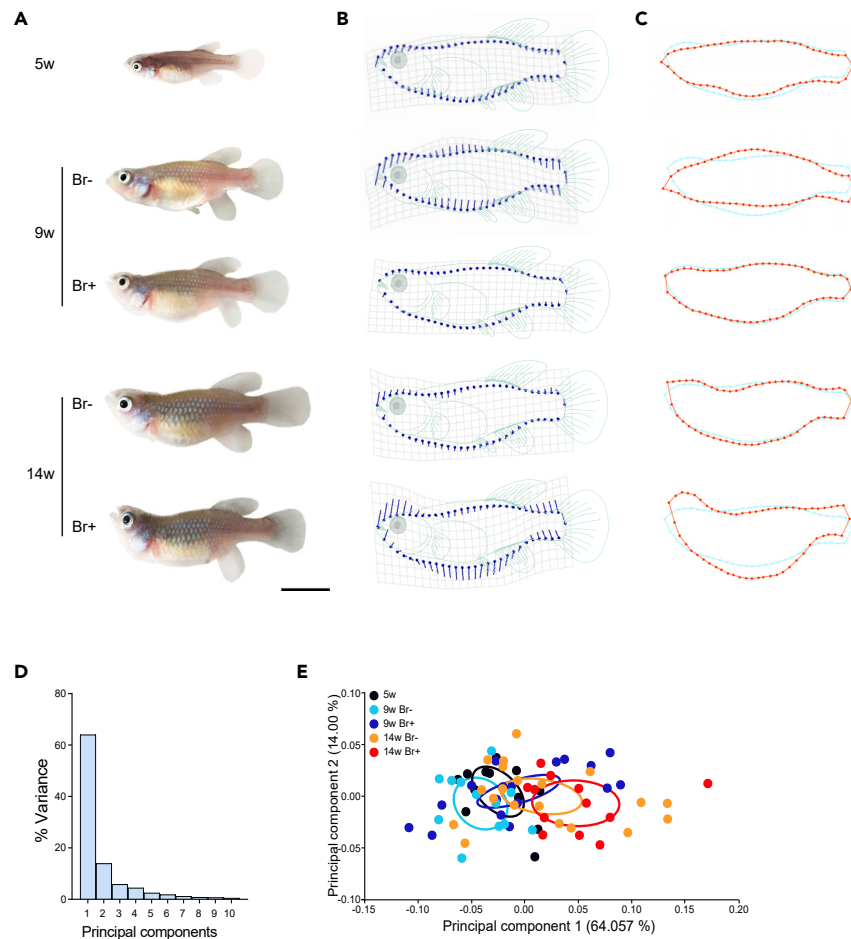


Figure 1. Quantitative analysis of body shape in female fish with respect to age and breeding status

(A) Representative images of each experimental group. Br+ and Br- indicate fish with or without breeding, respectively. Scale bar represents 1 cm.

(B) Body shape differences with respect to the average shape of all female fish were measured. Blue dots represent the average position of landmarks, and lines connected to blue dots indicate the direction and magnitude of alterations in shape, irrespective of fish size.

(C) Average body shape in each experimental group. Pale blue dots with lines indicate the average shape of all female fish, and red dots with lines indicate the average body shape in each experimental group.

(D) Principal component analysis (PCA) of body shape parameters.

(E) Distribution of experimental groups along PC1 and PC2. Solid lines indicate confidence ellipses for means (probability, 0.9) of each group. Each solid dot indicates an individual (5-week-old fish, $n = 12$; 9-week-old fish (Br-), $n = 12$; 9-week-old fish (Br+), $n = 17$; 14-week-old fish (Br-), $n = 20$; 14-week-old fish (Br+), $n = 12$). See also [Figures S1–S3](#).

Interestingly, spawning activity had a large impact on the BV/TV ratio, and this was more prominent in VOI1 than in VOI2 ([Figure 4B](#)). The increase in the BV/TV ratio in Weberian vertebrae was significantly attenuated in 9- and 14-week-old fish but not in caudal vertebrae.

Vertebrae architecture altered upon aging and spawning

To investigate further the difference in the BV/TV ratio between Weberian and caudal vertebrae ([Figure 4](#)), we examined the morphology and properties of a single caudal vertebra (vertebra number 14). The first caudal vertebrae (FCV) anatomy of the turquoise killifish was defined in sagittal and transverse micro-CT images and by reconstructing three-dimensional volume images ([Figure S5A](#), red-colored arrowhead; [Figures S5B–S5D](#)). Three-dimensional volume images of the turquoise killifish FCV revealed cortical bone (yellow-colored) and a tissue region (orange-colored) covered by cortical tissue, neural arch (NA), and hemal arch (HA) (magenta-colored), but the trabecular bone could not be clearly defined ([Figure S5B](#), [Video S2](#)). The thickness of the FCV bone of 14-week-old female fish with breeding was thinner, and the cortical bone was shorter in length, biased toward the center of the centrum, and rough on the centrum surface. The cortical bone also showed additional growth ([Figures S5C and S5D](#), [Video S3](#)). The intervertebral spaces between the first and second caudal vertebrae in 14-week-old female fish without breeding were clearly observed, and the vertebrae were regularly distributed; however, breeding severely reduced

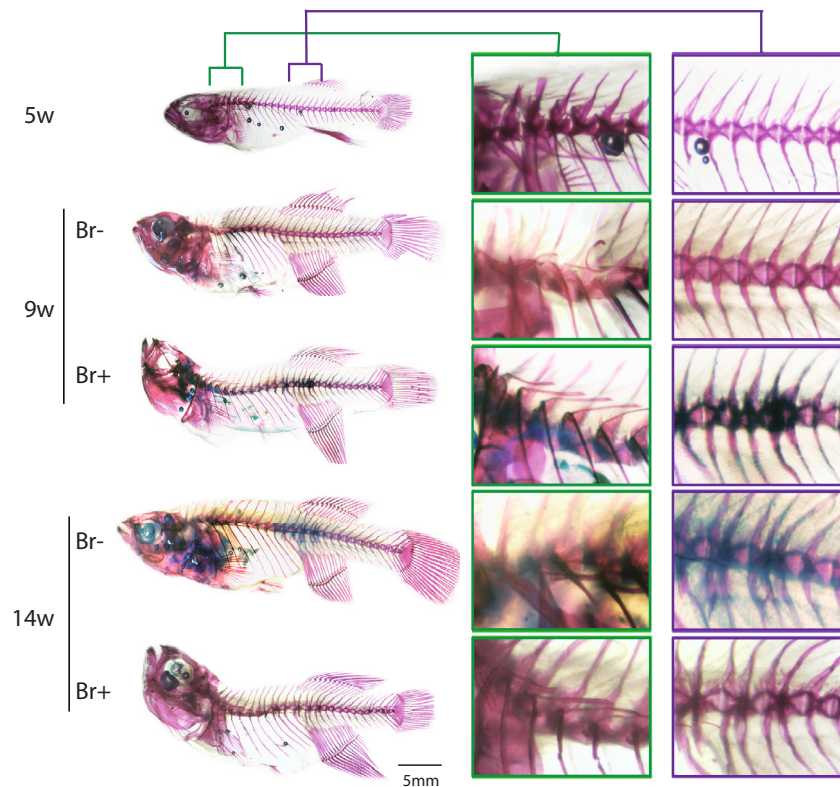


Figure 2. Whole bone staining revealed age- and reproductive activity-dependent deformation of the spine

Enlarged images in green and purple boxes show spinal regions near the head and caudal fin, respectively. See also [Figure S4](#).

the intervertebral space ([Figure 5A](#), [Video S3](#)). Aging resulted in the disruption of gaps between vertebrae around the FCV, which was more severe in breeding fish. This disruption included changes in vertebrae shape, array, and alignment.

Quantitative analysis of the FCV was performed ([Figure 5B](#)). The BV/TV ratio of the FCV provided us with results that were consistent with the BV/TV of VOI1 as shown in [Figure 4B](#). Specifically, the BV/TV ratio increased with fish aging and decreased during spawning activity. The cortical thickness (Ct.Th) in the FCV gradually increased with age, reaching a maximum of $41.9 \pm 4.8 \mu\text{m}$ in 14-week-old fish. However, this thickness was much lower in 14-week-old fish that were breeding, measuring only $27.2 \pm 2.4 \mu\text{m}$ ([Figure 5B](#)). The BMD increased in 9-week-old fish, but it did not show significant differences with age regardless of spawning activity in 9- and 14-week-old fish. FCV length, centrum radius, and NA and HA areas in the FCV of 9- and 14-week-old fish were significantly higher than those of 5-week-old fish; this increase was also suppressed by spawning activity. Interestingly, the NA area, but not the HA area, in the FCV expanded in 14-week-old female fish irrespective of spawning. The angles of the NA and HA in the FCV of 9- and 14-week-old female fish were significantly higher in fish with spawning.

Mineral contents of the turquoise killifish scale were correlated with BV/TV of vertebrae

To further estimate bone properties during fish aging and breeding in a less invasive manner, we measured mineralization in turquoise killifish scales by staining with calcein, a fluorescence dye for skeletal structure labeling²⁵ ([Figure 6](#)). Fluorescence intensities in aged turquoise killifish scales were more intense than those in young turquoise killifish, indicating increased scale mineralization in aged fish. Spawning fish exhibited lower fluorescence intensities than non-spawning fish at 9 and 14 weeks, as well as a reduction in scale size. The level of calcein staining was highly correlated with FCV characteristics such as BV/TV, Ct.Th, FCV length, and centrum radius.

Gene expression markers for estimating bone aging

To identify molecular markers for bone aging and vertebral collapse during aging and breeding, we evaluated genes in pathways involved in bone homeostasis that are known in mammalian models but not in turquoise killifish, such as RANK-RANKL-OPG, WNT/ β -catenin, and endochondral ossification pathways. Additionally, we evaluated vitamin D receptor (*vdr*) and estrogen receptor α (*esr1*), the most extensively studied genes in bone homeostasis and BMD. To find markers for spinal stenosis, we collected skeletal muscle just above the 1st to 6th vertebrae ([Figure S5](#)). The expression levels of *vdr* and *esr1* did not differ significantly with respect to age and breeding status ([Figure 7A](#)). In further analysis of 25 genes belonging to RANK-RANKL-OPG ([Figure 7B](#); [Figure S7A](#)), WNT/ β -catenin ([Figure 7C](#); [Figure S7B](#)), and endochondral ossification ([Figure 7D](#)) pathways, we observed highly complex patterns. We detected significant changes in expression with 1) age, 2)

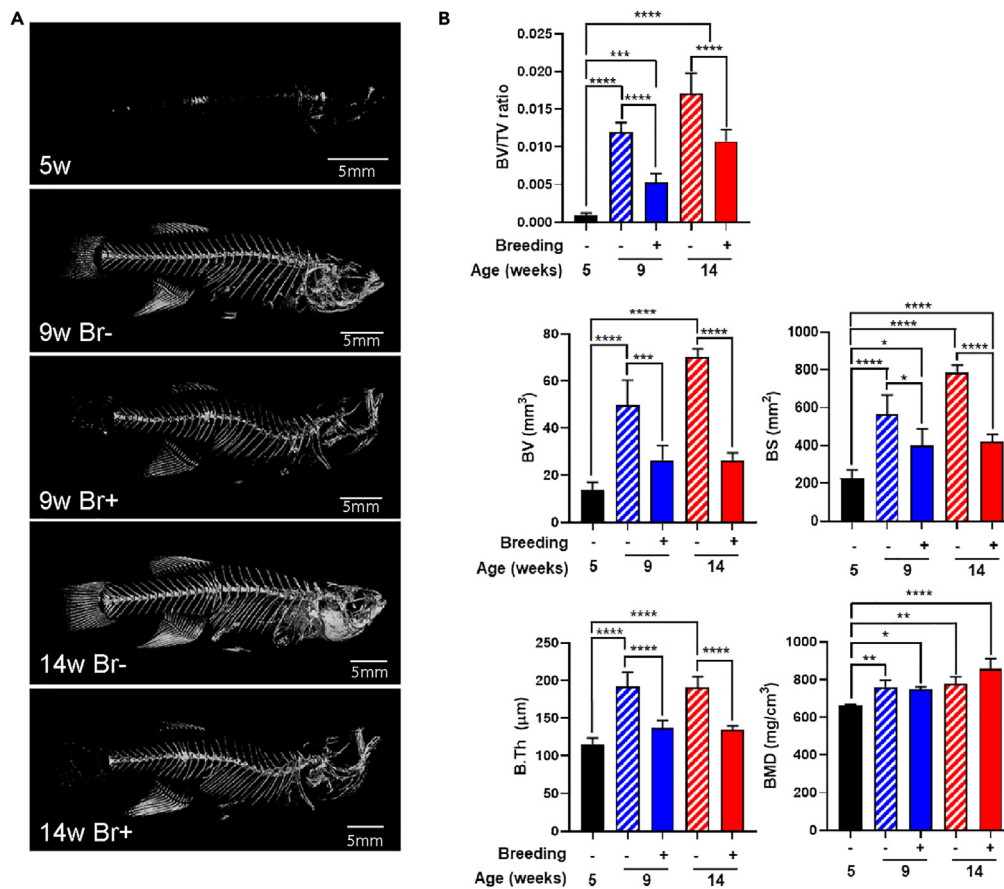


Figure 3. Breeding attenuates the age-related increase in bone volume in the turquoise killifish

(A) Representative micro-CT images.

(B) Bone parameters, including bone volume/tissue volume (BV/TV) ratio, bone volume (BV), bone surface (BS), average bone thickness (B.Th), and bone mineral density (BMD), were analyzed. Six fish were used for each group. Data represent the mean \pm SD from more than three biological trials; * $p < 0.05$, ** $p < 0.01$, *** $p < 0.001$, and **** $p < 0.0001$ compared to each group. See also [Video S1](#).

breeding, and 3) both age and breeding. For example, *sp7* and *sox9b* levels differed substantially between age groups and decreased significantly at 5 weeks after hatching. *sox9b* expression decreased further in fish with spawning (Figure 7D). The expression levels of *axin1* and *wnt4b* were significantly lower in spawning fish than in the non-spawning group and did not differ with aging (Figure 7C). Lastly, *tnfrsf11a* (encoding RANK), *wnt4a*, and *mef2ca* expression levels varied with age and breeding status (Figures 7B and 7C). In particular, *mef2ca* expression increased significantly during aging and was suppressed upon breeding. These results suggest that the expression of several genes is strongly correlated with bone aging, suggesting that they could be used as diagnostic markers of bone aging and vertebral collapse.

DISCUSSION

Bone tissue is complex, comprising multiple cell types and functions related to mineral storage. Age-associated bone weakness is linked to an increased risk of bone fractures and represents a significant concern within the elderly population. These age-related changes involve the dysregulation of bone remodeling, characterized by reduced bone formation and increased osteoclast activity. However, the relationship between bone homeostasis and spinal stenosis, as well as the underlying molecular mechanisms, remains unclear. We evaluated turquoise killifish as a potential model for studying age- and reproduction-associated spinal stenosis. Spinal curvature is a distinct and observable change associated with aging in the turquoise killifish, supported by the results of quantitative geometric morphometrics analysis (Figure 1). The vector movement of landmarks along the fish's body strongly suggests that precaudal vertebrae are the weakest segment of the fish spine. The comprehensive analysis of the entire spinal architecture further revealed curvature in the precaudal vertebrae during the aging process, particularly in response to breeding (Figure 2). Importantly, vertebral collapse around the dorsal and anal fins was clearly detected in response to aging and breeding. This vertebral collapse was notably more severe during the aging process, regardless of breeding status. Spinal stenosis by vertebral collapse in caudal vertebrae could be attributed to swimming behavior.

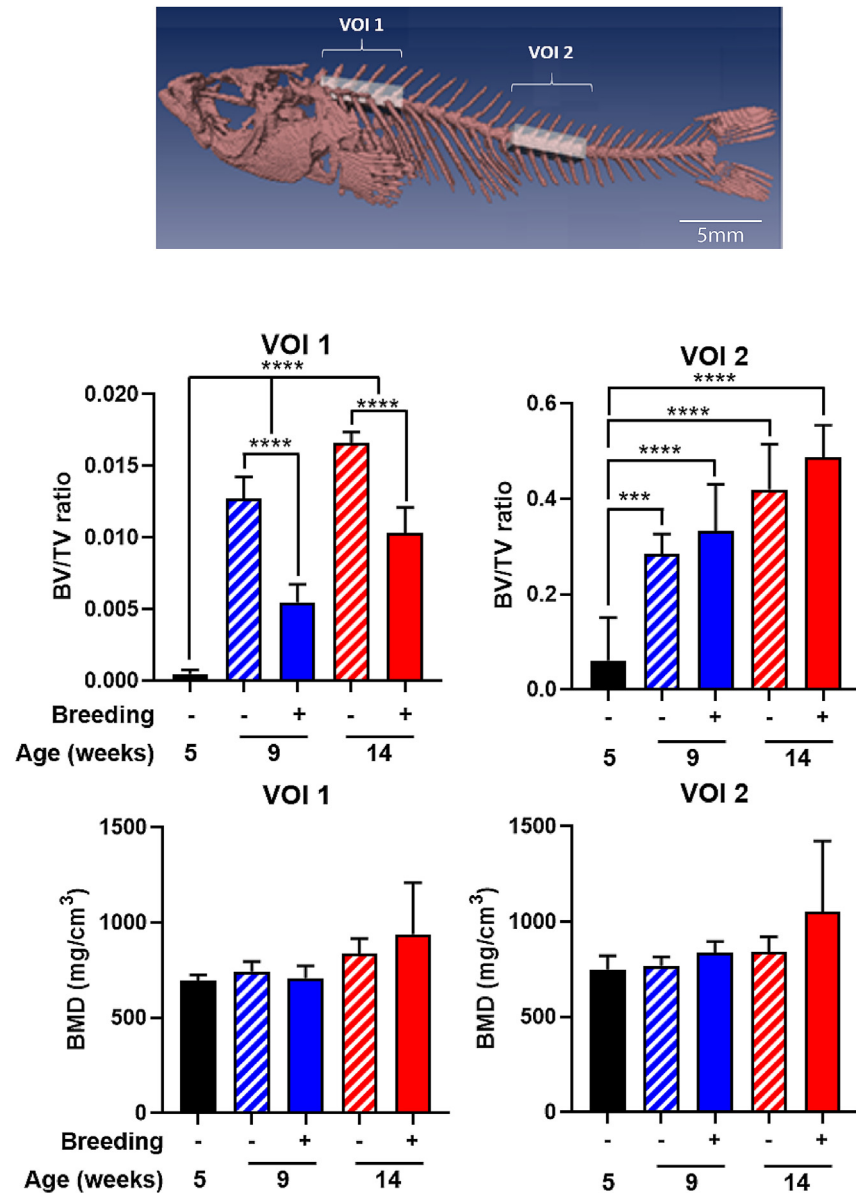


Figure 4. Increases in the BV/TV ratio and BMD of abdominal and caudal vertebrae with aging in female fish

Morphological images and parameters of abdominal and caudal vertebrae in the turquoise killifish are shown. Data represent the mean \pm SD of four females per experimental group. BMD, bone mineral density; BV/TV ratio, bone volume/tissue volume ratio. * $p < 0.05$, ** $p < 0.01$, *** $p < 0.001$, and **** $p < 0.0001$. See also [Video S2](#).

Aging leads to spinal stenosis before curvature becomes apparent, and reproductive activity accelerates spinal stenosis in both precaudal and caudal vertebrae. The altered body shape and whole bone staining results were recapitulated in an analysis of bone architecture by X-ray-based micro-CT (Figures 3, 4, and 5). X-ray-based tomography revealed fish age- and breeding-dependent changes in BMD, bone volume, cortical bone thickness, periosteal perimeter, centrum radius, NA and HA areas, and vertebral body length. In addition, FCV analysis revealed the presence of marginal osteophytes, which are well-known symptoms of osteoarthritis and one of the main causes of spinal stenosis. Osteophytes in turquoise killifish vertebrae were observed as rough surfaces in the transverse plane of the FCV, indicating that fish aging and breeding result in severe osteoarthritis (right panel of Figure S6D, Video S2 and S3). Interestingly, these phenotypes also correlated with fish age and reproductive activity but not with BMD. By contrast, BMD decreases during human bone aging, and spinal stenosis is often associated with aging; however, not all patients show these features, suggesting that BMD maintenance and spinal stenosis are independently regulated. In turquoise killifish bone aging, the collapsing of vertebrae together with sclerotic spinal bone could be one of the reasons for the increased BMD in fish with severe spinal stenosis.

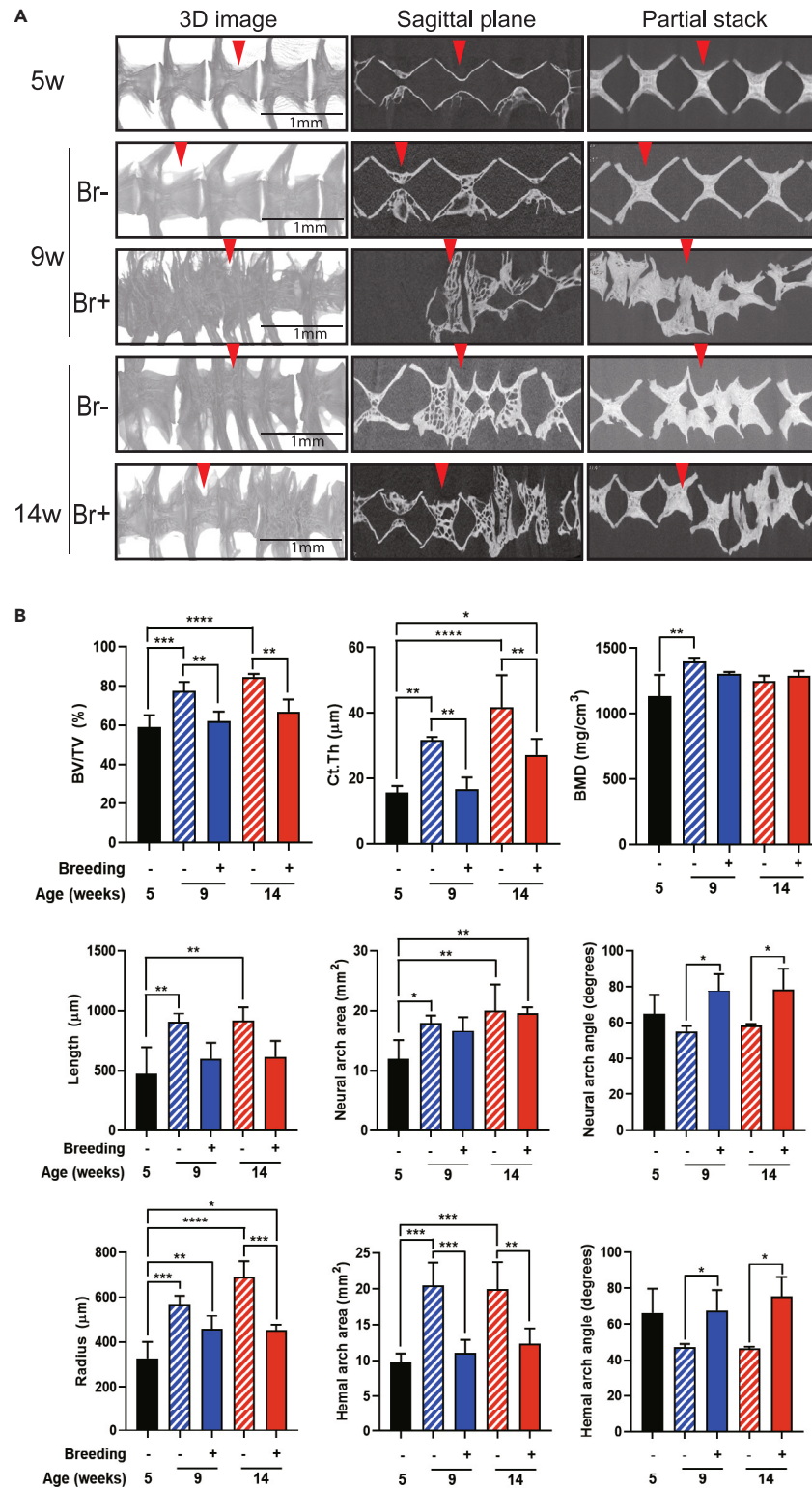


Figure 5. Vertebral images and vertebral bone measurements of the first caudal vertebrae (FCV) in aged and breeding fish

(A) Images of vertebrae were captured near the FCV (red marks) of aged and breeding fish. The images include 3-dimensional projections, single sagittal planes, and partially stacked sagittal plane images.

Figure 5. Continued

(B) Bone morphometric analysis of the FCV. Data represent the mean \pm SD of four individual females per experimental group. BMD, bone mineral density; BV, bone volume; BV/TV, bone volume fraction; Ct.Th, average cortical thickness; The length, radius, neural arch area, hemal arch area, neural arch angle, and hemal arch angle were measured using Dragonfly Pro software. * $p < 0.05$, ** $p < 0.01$, *** $p < 0.001$, and **** $p < 0.0001$. See also [Figure S5](#) and [Video S3](#).

Biomarkers of vertebral collapse will be critical for elucidating its molecular pathways and determining the efficacy of new treatments. Calcein staining is a useful method for assessing mineralization.²⁵ We found that mineralization of fish scales increased with age and decreased with breeding. However, BMD, spinal stenosis, and bone aging were decoupled in the turquoise killifish. We further searched for gene expression patterns mirroring the structural characteristics of fish spines. We evaluated 23 genes involved in bone homeostasis signaling pathways in skeletal muscle tissues adjacent to precaudal vertebrae. The decoupling of age- and reproduction-dependent bone properties was observed, as evaluated by BMD, spinal stenosis, cortical thickness, and trabecular number. Importantly, the expression levels of *tnfrsf11a* (encoding RANKL), *sost*, and *runx2* were reduced in female fish with aging or breeding, consistent with findings in mammalian osteoporosis, which were attributed to a decrease in osteoblast number.^{26,27} The results of gene expression analysis suggested that 1) molecular pathways associated with vertebral collapse can be separated by aging- and reproductive status-dependent responses, or 2) sensitivity to changes in bone homeostasis differ between pathways. For example, *sp7* and *sox9b* versus *axin1* and *wnt4b* show distinct aging- and reproduction-dependent expression changes. Furthermore, *sp7* and *sox9b* are early-responsive genes during aging, and *tnfrsf11a* is a late-responsive gene in age-dependent bone aging. Multiple observations throughout the fish life stages and systematic analyses of gene expression will be necessary to develop a concrete understanding of the molecular pathways underlying bone senescence.

In conclusion, turquoise killifish could be a powerful model for studies of bone diseases, especially spinal stenosis, during natural aging. Our results provide insights into the target region of spinal stenosis in the turquoise killifish, detailed information about the bone architecture during aging and reproduction, and candidate gene expression markers for spinal stenosis.

Limitations of the study

Aging and reproductive activity in the female killifish are highly associated with vertebral collapse in this study. Micro-CT images of vertebrae also revealed severe deformation and osteophytes formation in aged female killifish. The evidence presented in this study indicates that turquoise killifish undergo age- and reproductive activity-dependent spinal stenosis, similar to what is often observed in humans. However, it is important to note that turquoise killifish serve as a nonhuman model organism; thus, the phenotypes observed in this model must be translated to those relevant to humans. The most notable common features between human and killifish bone alterations during aging and reproductive activity include vertebral collapse, osteoarthritis, and osteophytes formation. These shared phenotypes provide valuable insights that can be investigated to develop treatments for conditions such as spinal stenosis and bone aging.

Gene expression markers were investigated in correlation with spinal stenosis in female killifish. These genes were tested within adjacent muscle tissue near the spine rather than directly within the spine. A significant proportion of these genes exhibited correlation with the vertebral collapse phenotype. Further classification was conducted to determine whether they were associated with aging, reproduction, or both. This suggests that gene expression tests from adjacent muscle tissue near the spine can potentially be used for monitoring spinal stenosis.

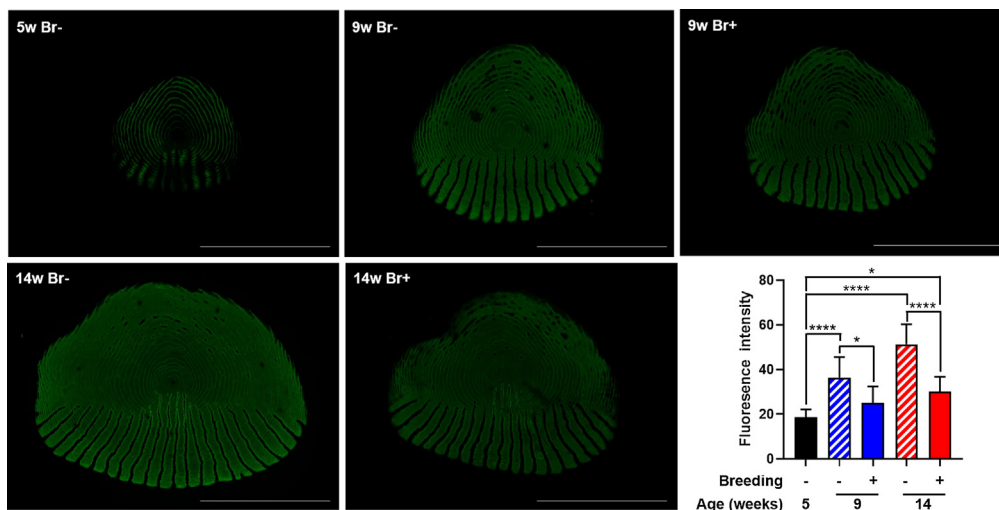


Figure 6. Mineralization of the turquoise killifish scale

The scales ($n = 10$) were collected and stained with calcein solution for 15 min. The stained scales were photographed using an LSM 700 Zeiss confocal laser scanning microscope. The mineralized area was quantified using ImageJ analysis of images of fluorescent calcein staining. All results are expressed as the mean \pm SD of more than three individual experiments; * $p < 0.05$, and **** $p < 0.0001$.

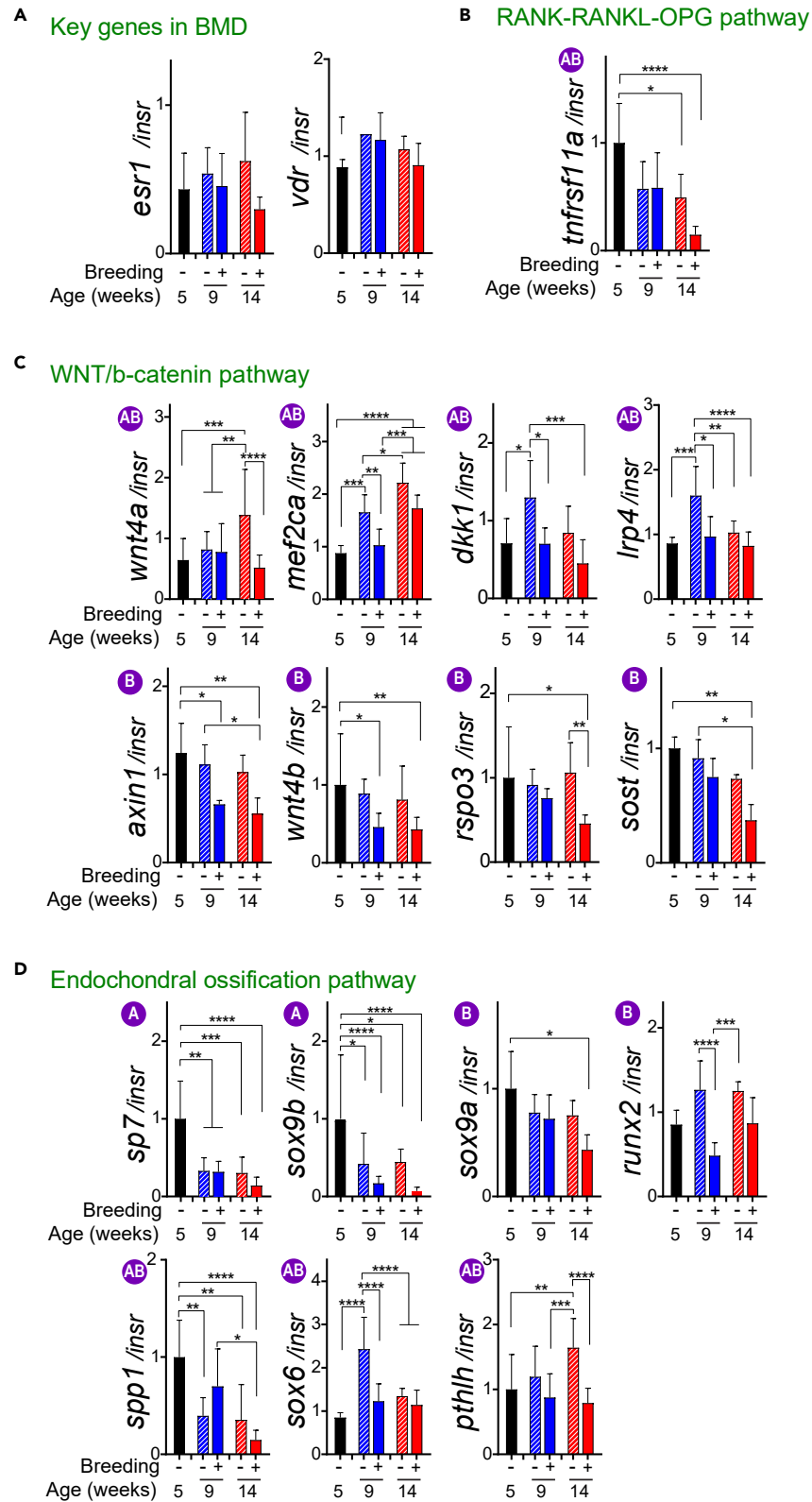


Figure 7. Expression of bone aging marker candidates

(A–D) Expression of key genes in the BMD (A), RANK-RANKL-OPG (B), WNT/ β -catenin (C), and endochondral ossification pathways (D). Genes in purple circles represent those showing aging-dependent and/or breeding-dependent expression patterns. Data are expressed as means \pm SD from six individual females per experimental group. * $p < 0.05$, ** $p < 0.01$, *** $p < 0.001$, and **** $p < 0.0001$ as determined by one-way ANOVA followed by Tukey’s multiple comparison tests. See also [Figures S5](#) and [S6](#).

STAR★METHODS

Detailed methods are provided in the online version of this paper and include the following:

- [KEY RESOURCES TABLE](#)
- [RESOURCE AVAILABILITY](#)
 - Lead contact
 - Materials availability
 - Data and code availability
- [EXPERIMENTAL MODEL AND STUDY PARTICIPANT DETAILS](#)
- [METHOD DETAILS](#)
 - Fish husbandry
 - Quantification of fish body shape
 - Alizarin red S staining
 - Micro-CT imaging and bone analysis
 - Calcein staining
 - Bone homeostasis gene marker expression
- [QUANTIFICATION AND STATISTICAL ANALYSIS](#)

SUPPLEMENTAL INFORMATION

Supplemental information can be found online at <https://doi.org/10.1016/j.isci.2023.107877>.

ACKNOWLEDGMENTS

This work was supported by the Institute for Basic Science, Daegu, Republic of Korea (IBS-R013-D1 and IBS-R022-D1), the Korea Institute of Oriental Medicine, Ministry of Education, Science and Technology, Republic of Korea (SN2013330, W21003 to JIP), the National Research Foundation of Korea (NRF) grant funded by the Korea government (MSIT) (No. NRF-2020R1A2C1008527), and the Promotion of Innovative Businesses for Regulation-Free Special Zones funded by the Ministry of SMEs and Startups (No. 1425157301).

AUTHOR CONTRIBUTIONS

Y.K. and K.-N.K. conceived and designed the project. S.-H.C., S.L., N.G., Y.L.Y., S.-R.K., J.A., H.J., S.Y.K., and Y.K. performed experiments. S.-H.C., S.-R.K., Y.L.Y., H.-Y.J., and J.-I.P. provided technical assistance for micro-CT and sub-micro-CT analysis. Y.K., S.-H.C., J.-I.P., and K.-N.K. wrote the manuscript. All authors read and adjusted the manuscript.

DECLARATION OF INTERESTS

The authors declare no competing interests.

Received: September 28, 2022

Revised: March 22, 2023

Accepted: September 7, 2023

Published: September 9, 2023

REFERENCES

1. Singh, A., Dutta, M.K., Jennane, R., and Lespessailles, E. (2017). Classification of the trabecular bone structure of osteoporotic patients using machine vision. *Comput. Biol. Med.* 91, 148–158. <https://doi.org/10.1016/j.combiomed.2017.10.011>.
2. Suarez-Bregua, P., Torres-Nuñez, E., Saxena, A., Guerreiro, P., Braasch, I., Prober, D.A., Moran, P., Cerda-Reverter, J.M., Du, S.J., Adrio, F., et al. (2017). Pth4, an ancient parathyroid hormone lost in eutherian mammals, reveals a new brain-to-bone signaling pathway. *FASEB J.* 31, 569–583. <https://doi.org/10.1096/fj.201600815R>.
3. Tiede-Lewis, L.M., Xie, Y., Hulbert, M.A., Campos, R., Dallas, M.R., Dusevich, V., Bonewald, L.F., and Dallas, S.L. (2017). Degeneration of the osteocyte network in the C57BL/6 mouse model of aging. *Aging* 9, 2190–2208. <https://doi.org/10.18632/aging.101308>.
4. Castelein, R.M., van Dieën, J.H., and Smit, T.H. (2005). The role of dorsal shear forces in the pathogenesis of adolescent idiopathic scoliosis—a hypothesis. *Med. Hypotheses* 65, 501–508. <https://doi.org/10.1016/j.mehy.2005.03.025>.
5. Raja, A., Hoang, S., Patel, P., and Mesfin, F.B. (2021). *Spinal Stenosis (StatPearls)*.
6. Hunter, D.J., Gerstenfeld, L., Bishop, G., Davis, A.D., Mason, Z.D., Einhorn, T.A., Maciewicz, R.A., Newham, P., Foster, M.,

- Jackson, S., and Morgan, E.F. (2009). Bone marrow lesions from osteoarthritis knees are characterized by sclerotic bone that is less well mineralized. *Arthritis Res. Ther.* 11, R11. <https://doi.org/10.1186/ar2601>.
7. Florencio-Silva, R., Sasso, G.R.d.S., Sasso-Cerri, E., Simões, M.J., and Cerri, P.S. (2015). Biology of Bone Tissue: Structure, Function, and Factors That Influence Bone Cells. *BioMed Res. Int.* 2015, 421746. <https://doi.org/10.1155/2015/421746>.
8. Lacey, D.L., Timms, E., Tan, H.L., Kelley, M.J., Dunstan, C.R., Burgess, T., Elliott, R., Colombero, A., Elliott, G., Scully, S., et al. (1998). Osteoprotegerin ligand is a cytokine that regulates osteoclast differentiation and activation. *Cell* 93, 165–176. [https://doi.org/10.1016/S0092-8674\(00\)81569-X](https://doi.org/10.1016/S0092-8674(00)81569-X).
9. Li, J., Sarosi, I., Yan, X.Q., Morony, S., Capparelli, C., Tan, H.L., McCabe, S., Elliott, R., Scully, S., Van, G., et al. (2000). RANK is the intrinsic hematopoietic cell surface receptor that controls osteoclastogenesis and regulation of bone mass and calcium metabolism. *Proc. Natl. Acad. Sci. USA* 97, 1566–1571. <https://doi.org/10.1073/pnas.97.4.1566>.
10. Boyle, W.J., Simonet, W.S., and Lacey, D.L. (2003). Osteoclast differentiation and activation. *Nature* 423, 337–342. <https://doi.org/10.1038/nature01658>.
11. Rauner, M., Sipos, W., and Pietschmann, P. (2008). Age-dependent Wnt gene expression in bone and during the course of osteoblast differentiation. *Age* 30, 273–282. <https://doi.org/10.1007/s11357-008-9069-9>.
12. Stevens, J.R., Miranda-Carboni, G.A., Singer, M.A., Brugger, S.M., Lyons, K.M., and Lane, T.F. (2010). Wnt10b Deficiency Results in Age-Dependent Loss of Bone Mass and Progressive Reduction of Mesenchymal Progenitor Cells. *J. Bone Miner. Res.* 25, 2138–2147. <https://doi.org/10.1002/jbmr.118>.
13. Matsubara, T., Kida, K., Yamaguchi, A., Hata, K., Ichida, F., Meguro, H., Aburatani, H., Nishimura, R., and Yoneda, T. (2008). BMP2 Regulates Osterix through Msx2 and Runx2 during Osteoblast Differentiation. *J. Biol. Chem.* 283, 29119–29125. <https://doi.org/10.1074/jbc.M801774200>.
14. Lescaq, E.A., and Milligan-Myhre, K.C. (2017). Teleosts as Model Organisms To Understand Host-Microbe Interactions. *J. Bacteriol.* 199, e00868–16. <https://doi.org/10.1128/JB.00868-16>.
15. Laize, V., Gavaia, P.J., Leonor, M., and Cancela, L. (2014). Fish: a suitable system to model human bone disorders and discover drugs with osteogenic or osteotoxic activities. *Drug Discov. Today Dis. Model.* 13, 26–37. <https://doi.org/10.1016/j.ddmod.2014.08.001>.
16. Kim, Y., Nam, H.G., and Valenzano, D.R. (2016). The short-lived African turquoise killifish: an emerging experimental model for ageing. *Dis. Model. Mech.* 9, 115–129. <https://doi.org/10.1242/dmm.023226>.
17. Suniaga, S., Rolvien, T., vom Scheidt, A., Fiedler, I.A.K., Bale, H.A., Huysseune, A., Witten, P.E., Amling, M., and Busse, B. (2018). Increased mechanical loading through controlled swimming exercise induces bone formation and mineralization in adult zebrafish. *Sci. Rep.* 8, 3646. <https://doi.org/10.1038/s41598-018-21776-1>.
18. Hur, M., Gistelink, C.A., Huber, P., Lee, J., Thompson, M.H., Monstad-Rios, A.T., Watson, C.J., McMenamin, S.K., Willaert, A., Parichy, D.M., et al. (2017). MicroCT-based phenomics in the zebrafish skeleton reveals virtues of deep phenotyping in a distributed organ system. *Elife* 6, e26014. <https://doi.org/10.7554/eLife.26014>.
19. Yu, L.L., Tucci, V., Kishi, S., and Zhdanova, I.V. (2006). Cognitive Aging in Zebrafish. *PLoS One* 1. <https://doi.org/10.1371/journal.pone.0000014>.
20. Khajuria, D.K., and Karasik, D. (2021). Novel model of restricted mobility induced osteopenia in zebrafish. *J. Fish. Biol.* 98, 1031–1038. <https://doi.org/10.1111/jfb.14369>.
21. Monma, Y., Shimada, Y., Nakayama, H., Zang, L., Nishimura, N., and Tanaka, T. (2019). Aging-associated microstructural deterioration of vertebra in zebrafish. *BoneKey Rep.* 11, 100215. <https://doi.org/10.1016/j.bonr.2019.100215>.
22. Terzibas, E., Valenzano, D.R., Benedetti, M., Roncaglia, P., Cattaneo, A., Domenici, L., and Cellerino, A. (2008). Large differences in aging phenotype between strains of the short-lived annual fish *Nothobranchius furzeri*. *PLoS One* 3, e3866. <https://doi.org/10.1371/journal.pone.0003866>.
23. Tozzini, E.T., Baumgart, M., Battistoni, G., and Cellerino, A. (2012). Adult neurogenesis in the short-lived teleost *Nothobranchius furzeri*: localization of neurogenic niches, molecular characterization and effects of aging. *Aging Cell* 11, 241–251. <https://doi.org/10.1111/j.1474-9726.2011.00781.x>.
24. Di Cicco, E., Tozzini, E.T., Rossi, G., and Cellerino, A. (2011). The short-lived annual fish *Nothobranchius furzeri* shows a typical teleost aging process reinforced by high incidence of age-dependent neoplasias. *Exp. Gerontol.* 46, 249–256. <https://doi.org/10.1016/j.exger.2010.10.011>.
25. Rahn, B.A., and Perren, S.M. (1971). Xylenol Orange, a Fluorochrome Useful in Polychrome Sequential Labeling of Calcifying Tissues. *Stain Technol.* 46, 125–129. <https://doi.org/10.3109/10520297109067836>.
26. Sebastian, A., and Loots, G.G. (2017). Transcriptional control of *Sost* in bone. *Bone* 96, 76–84. <https://doi.org/10.1016/j.bone.2016.10.009>.
27. Pérez-Campo, F.M., Santurtún, A., García-Ibarbia, C., Pascual, M.A., Valero, C., Garcés, C., Sañudo, C., Zarrabeitia, M.T., and Riancho, J.A. (2016). Osterix and RUNX2 are Transcriptional Regulators of Sclerostin in Human Bone. *Calcif. Tissue Int.* 99, 302–309. <https://doi.org/10.1007/s00223-016-0144-4>.
28. Lee, S., Nam, H.G., and Kim, Y. (2021). The core circadian component, *Bmal1*, is maintained in the pineal gland of old killifish brain. *iScience* 24, 101905. <https://doi.org/10.1016/j.iisci.2020.101905>.
29. Klingenberg, C.P. (2011). MorphoJ: an integrated software package for geometric morphometrics. *Mol. Ecol. Resour.* 11, 353–357. <https://doi.org/10.1111/j.1755-0998.2010.02924.x>.
30. Hartmann, N., Reichwald, K., Wittig, I., Dröse, S., Schmeisser, S., Lück, C., Hahn, C., Graf, M., Gausmann, U., Terzibas, E., et al. (2011). Mitochondrial DNA copy number and function decrease with age in the short-lived fish *Nothobranchius furzeri*. *Aging Cell* 10, 824–831. <https://doi.org/10.1111/j.1474-9726.2011.00723.x>.

STAR★METHODS

KEY RESOURCES TABLE

REAGENT or RESOURCE	SOURCE	IDENTIFIER
Experimental models: Organisms/strains		
GRZ-AD		
Chemicals, peptides, and recombinant proteins		
Ethyl 3-aminobenzoate methanesulfonate (Tricaine)	Sigma-Aldrich	E10521
4% paraformaldehyde	Biosesang	P2031
Potassium hydroxide	Sigma-Aldrich	306568
30% Hydrogen peroxide solution	Sigma-Aldrich	H1009
Alizarin red S	Sigma-Aldrich	A5533
Borax Anhydrous	Sigma-Aldrich	71997
Trypsin	Sigma-Aldrich	T4799
Glycerol	Sigma-Aldrich	G5516
Ethyl alcohol, anhydrous, 99.9%	SAMCHUN	E0690
Calcein solution	Sigma-Aldrich	C1359
RNAlater™	Invitrogen	AM7021
QIAzol Lysis Reagent	QIAGEN	79306
SuperScript™ IV VILOTM Master Mix with ezDNase™ Enzyme	Invitrogen	11766050
iTaq Universal SYBR Green Supermix	BIO-RAD	1725121
Oligonucleotides		
esr1-F: gccttctcaagaggagcatt	This study	N/A
esr1-R: ttctcggattcctgtcaat	This study	N/A
vdr-F: tgatgacctctgattcatt	This study	N/A
vdr-R: aacaggctgctgaggttcat	This study	N/A
axin1-F: agcacacggggtatagcaaa	This study	N/A
axin1-R: ggtcgaactcgtcacctt	This study	N/A
ctnnb1-F: aggtatcgaggcgttggtc	This study	N/A
ctnnb1-R: cagctggctctgtgatgtct	This study	N/A
dkk1-F: cccatgggtttcagccta	This study	N/A
dkk1-R: cagtctcactatccgtgcaaa	This study	N/A
gpr177-F: aaagaggaaactcactgcaac	This study	N/A
gpr177-R: aaacgaccatcgttcacgta	This study	N/A
jag1b-F: caccttcaccctaaacaagga	This study	N/A
jag1b-R: gagcctcagctgcttacaca	This study	N/A
lrp4-F: cgtatccacagggttgatga	This study	N/A
lrp4-R: tgtgtctgtccagtagaccttc	This study	N/A
lrp5-F: caaccgactgtgttacttc	This study	N/A
lrp5-R: ggaagagtgaacaccagga	This study	N/A
lrp6-F: aagctgttctgggtgactc	This study	N/A
lrp6-R: ttagagtcggcgatcacaatc	This study	N/A
mef2ca-F: tccaacaagtgcaccaaat	This study	N/A

(Continued on next page)

Continued

REAGENT or RESOURCE	SOURCE	IDENTIFIER
mef2ca-R: agccgtctgggagtgatt	This study	N/A
mef2cb-F: cagggcatgggtggttac	This study	N/A
mef2cb-R: gcactgttcaggaataactcg	This study	N/A
pthlh-F: ccggacctgagaacctgt	This study	N/A
pthlh-R: accacggcaagaaccagt	This study	N/A
rspo3-F: caggagagctgccagac	This study	N/A
rspo3-R: caccgggaacacactct	This study	N/A
sost-F: aaagacaatcgaatataaacacgctc	This study	N/A
sost-R: aggagcaaaaatacagaacacctt	This study	N/A
wnt16-F: agcatgaaccagcacaacag	This study	N/A
wnt16-R: tgtggacatcgctctctcaa	This study	N/A
wnt4a-F: gcagcagtgagagaactgga	This study	N/A
wnt4a-R: ggaagccctctggactgact	This study	N/A
wnt4b-F: tggcagagtgaaccaag	This study	N/A
wnt4b-R: ctgctgaggacagagcatga	This study	N/A
wnt5b-F: ccctcatgaacctgcacaat	This study	N/A
wnt5b-R: cgccatgacacttacaggaa	This study	N/A
tnfrsf11a-F: tgggggtcttaatgagcagt	This study	N/A
tnfrsf11a-R: gagcattgcctggctttaac	This study	N/A
tnfrsf11b-F: ctgactgtgcccgtactga	This study	N/A
tnfrsf11b-R: ccagaggcactgaggacag	This study	N/A
sox9a-F: taccgcacctccaac	This study	N/A
sox9a-R: cgcttctctctctgttcag	This study	N/A
sox9b-F: gcacaacgcagagctcagta	This study	N/A
sox9b-R: ctacgaacggacgcttctct	This study	N/A
runx2-F: ttcaatgatctctgctttgtg	This study	N/A
runx2-R: tgattgtcagcgtagaagctc	This study	N/A
sox6-F: ctgtggcctcaacaactg	This study	N/A
sox6-R: gctgatgtccaaggtgtca	This study	N/A
sp7-F: agggaatgtaattgtaaacacacg	This study	N/A
sp7-R: cgaattgttgaggtagca	This study	N/A
spp1-F: gggatcagacgagagctcag	This study	N/A
spp1-R: taccgcagcagcttgaact	This study	N/A

Software and algorithms

tpsDig2	Stony Brook University	Version 2.31,
MorphoJ	Klingenberg lab	version 1.07.a
Dragonfly Pro software	Object Research Systems	
Analyze 12.0 software	AnalyzeDirect	
GraphPad PRISM software version 8.0	GraphPad	version 8.0

Other

LSM 700 Zeiss confocal laser scanning microscope	Zeiss	
Micro-CT scanner	Zeiss	Xradia versa 620 imaging system
PerkinElmer's AccuCT™	Quality Assurance in Radiology and Medicine GmbH	QRM-Micro CT-HA

RESOURCE AVAILABILITY

Lead contact

Further information and requests for resources and reagents should be directed to and will be fulfilled by the lead contact, Yumi Kim (yumikim@unist.ac.kr).

Materials availability

This study did not generate new unique reagents.

Data and code availability

- All data reported in this paper will be shared by the [lead contact](#) upon request.
- This paper does not report original code.
- Any additional information required to reanalyze the data reported in this paper is available from the [lead contact](#) upon request.

EXPERIMENTAL MODEL AND STUDY PARTICIPANT DETAILS

Laboratory strain GRZ-AD (*Nothobranchius furzeri*) is used in this study. Fish husbandry and experiments were performed according to an animal care and use protocol that was reviewed and approved by the Institutional Animal Care and Use Committee at Daegu Gyeongbuk Institute of Science and Technology, Republic of Korea (Approval number: DGIST-IACUC-20112402-0000).

METHOD DETAILS

Fish husbandry

Only female GRZ-AD fish of 5-, 9-, and 14-week-old (corresponding to the times of sexual maturity, high reproductive activity, and median lifespan, respectively) were used. They were maintained under a 12-h light and 12-h dark cycle. The fish were singly housed in a 1.8 L tank before being transferred to a breeding tank.²⁸ At 6 weeks after hatching, we placed one male and two females that had hatched on the same day in a breeding tank. Female fish were sacrificed at 5 weeks old, 9 weeks old (with or without breeding), and 14 weeks old (with or without breeding). The number of fish is indicated in each figure.

Quantification of fish body shape

After sacrifice, female fish were imaged with a scale bar before use. Fish images were processed to define landmarks along the fish body as follows. 1) The tips of the snout and body were defined first in an image of the fish in a horizontal position. 2) Then, two landmarks were placed on the same horizontal line, and 30 vertical guidelines that were evenly distributed between the snout and body tips were drawn. 3) The images were imported into tpsDig2 (Version 2.31, Stony Brook University) and 58 landmarks that crossed with the 30 guidelines were defined along the fish body line. 4) The images were saved as *.tps files and analyzed in MorphoJ (version 1.07.a).²⁹ Procrustes shape coordinates and wire-frame shapes derived from MorphoJ analysis were used in the figures.

Alizarin red S staining

The turquoise killifish were fixed with 4% paraformaldehyde (PFA; Biosesang, Korea) for 3 days and rinsed in distilled water overnight. The skin and internal organs of the rinsed killifish were removed carefully so as not to damage the ribs. The fish were then placed in 1% potassium hydroxide (KOH; Sigma Aldrich, USA) with 3% hydrogen peroxide (H₂O₂; Sigma Aldrich, USA) to bleach the pigment overnight. After rinsing in distilled water for 30 min, the fish were placed in saturated sodium borate overnight. Subsequently, the fish were stained with Alizarin red solution (1 mg/ml Alizarin red in 1% KOH) at room temperature overnight. Stained fish were rinsed in distilled water for 30 min and then placed in 1% trypsin in 2% borax overnight until tissue clearing. The fish were sequentially transferred to 20% and 40% glycerol diluted in 1% KOH. Finally, the fish were stored in 70% glycerol diluted in 70% ethanol until imaging. The samples were visualized using an LSM 700 Zeiss confocal laser scanning microscope (Zeiss, Germany). The number of vertebrae of the turquoise killifish was measured using 5-week-old fish and revealed that it is composed of 29 vertebrae ([Figure S4](#)).

Micro-CT imaging and bone analysis

After fixation, the whole body and caudal vertebrae of the killifish were scanned to evaluate morphological characteristics using a micro-CT scanner (Xradia versa 620 imaging system, Zeiss, Dublin, CA) at Korea Basic Science Institute (Gwangju, Korea). Samples were scanned in sample holders that oriented the samples vertically on the stage and rotated them horizontally by 180° + fan. For whole-body bone images, samples were placed 48 mm from the rotation axis (RA)-Source and 53 mm from the RA-detector. The bones were scanned at 30 μm resolution using a 0.4× objective with energy settings of 60 kV, 110 μA, and 6.5 W with an air filter and 601 projections. The first caudal vertebrae (FCV; vertebrate number 14) bear the centrum, neural spine, neural canal, neural arch (NA), hemal spine, hemal canal, and hemal arch (HA). For caudal vertebrae images, samples were placed 48 mm from the RA-Source and 63 mm from the RA-detector and scanned at 3 μm resolution using a 4× objective with the following settings:

80 kV, 125 μ A, 10 W, low energy 1 (LE1) filter, and 1,601 projections. Following scanning, the structural parameters of the bone were analyzed using Dragonfly Pro software (Object Research Systems, QC, Canada). To identify the bone region, segmentation using a paintbrush tool was performed to highlight regions only within a certain threshold range and relied on manual correction within Dragonfly. Cortical and trabecular bone were manually segmented in three dimensions using a global threshold for each sample. Bone volume/tissue volume (BV/TV) ratio, bone volume (BV), bone surface (BS), bone volume fraction (BV/TV), average bone thickness (B.Th) and average cortical thickness (Ct.Th) of whole bones or caudal vertebrae were automatically calculated using the ROI tool of Analyze 12.0 software (AnalyzeDirect, Overland Park, KS, USA) and Dragonfly. The BMD for the whole body, volume of interest (VOI) 1, VOI 2, and the first caudal vertebrae were analyzed by Analyze 12.0 software and PerkinElmer's AccuCT using a hydroxyapatite (HA) phantom (QRM-MicroCT-HA, Quality Assurance in Radiology and Medicine GmbH, Germany). A manual measurement tool in Dragonfly Pro software was used to calculate the length of the first caudal vertebrae, radius of centrum, neural and hemal arch angle, and neural and hemal arch area in two-dimensional projections of the vertebral body.

Calcein staining

The turquoise killifish scales were collected in 24-well plates after fixation of whole bodies and washed twice using distilled water. The scales were stained using 0.02% calcein solution (Sigma Aldrich, USA) for 15 min at room temperature in the dark. Stained scales were washed three times using fresh distilled water, placed on a glass slide, and analyzed using an LSM 700 Zeiss confocal laser scanning microscope (Zeiss, Germany) with laser excitation at 488 nm and emission at 490–555 nm using a band-pass filter.

Bone homeostasis gene marker expression

Sacrificed female fish from each experimental group were stored in RNAlater Stabilization Solution (AM7021, Invitrogen) until dissection. Skeletal muscle, posterior skull, and the upper spine where spinal curvature occurred were used for RNA isolation. Total RNA isolation and qRT-PCR were performed as described.²⁸ Briefly, skeletal muscle tissues were finely ground in liquid nitrogen. Total RNAs were extracted using QIAzol Lysis Reagent (79306, QIAGEN), and cDNAs were generated with ezDNaseTM Enzyme (11766050, Invitrogen) from 2.5 μ g of total RNA. After synthesis, the resulting cDNAs underwent a 10-fold dilution. Subsequently, 3 μ L of the diluted cDNA was used as the template for qPCR, employing the SsoAdvanced Universal SYBR Green Supermix from BioRad. The primers of candidate genes used are listed below, and gene expression was normalized to *insr* expression, which is known to remain constant over fish age.³⁰

Gene Name	Gene Identifier	Position	Forward Primer	Reverse Primer
<i>esr1</i>	Nfu_g_1_018896	sgr04:46956170.46959652 (-)	gccttctcaagaggagcatt	ttctccgattctgtcaat
<i>vdr</i>	Nfu_g_1_001579	sgr15:35277926.35360575 (+)	tgatgctctctgattcatt	aacaggctgctgagggtcat
<i>axin1</i>	Nfu_g_1_007729	sgr05:5057477.5080925 (+)	agcacacggggtatagcaaa	ggctgaactctgacacctt
<i>ctnbn1</i>	Nfu_g_1_001773	sgr05:23456531.23466969 (-)	aggatcagaggcgttggtc	cagctggctctgtgatgct
<i>dkk1</i>	Nofu_GRZ_cDNA_3_0038409	sgr03:36905916.37002563 (-)	cccatgggttcagccta	cagttctactatccgtgcaaa
<i>gpr177</i>	Nfu_g_1_017967	scaffold00098:47984.85535 (-)	aaagagaaactcactgcaac	aaacgacctctgtcactgta
<i>jag1b</i>	Nfu_g_1_016084	sgr03:1345858.1373531 (+)	caccttcaccctaacaagga	gagcctcagctgcttacaca
<i>lrp4</i>	Nfu_g_1_003223	sgr07:30376839.30531972 (-)	cgatccacaggggtgatga	tgtgtctgctcagtagaccttc
<i>lrp5</i>	Nfu_g_1_005969	sgr14:6816949.6864710 (+)	caaccgactgtgttacttc	ggaagagtggaacaccagga
<i>lrp6</i>	Nfu_g_1_011995	sgr01:96327452.96375472 (+)	aagctgttctgggtggactc	ttagagctggcgatcacaatc
<i>mef2ca</i>	Nfu_g_1_010849	sgr02:33490300.33537707 (-)	tccaacaagtgcaccaacat	agccgtctgggagtgattt
<i>mef2cb</i>	Nfu_g_1_009457	sgr18:19378798.19452695 (+)	cagggatgggtggttac	gactgttcagggaataactcg
<i>pthlh</i>		GapFilledScaffold_1782:40906.54180	ccggacctgagaacctgt	accacggcaagaaccagt
<i>rspo3</i>	Nfu_g_1_001794	sgr05:24037880.24050291 (+)	caggagagctgccagac	caccgggaacactct
<i>sost</i>	Nfu_g_1_023062	sgr12:14353217.14355224 (-)	aaagacaaatcgaataaacacgtc	aggagcaaaaatacagaacacctt
<i>wnt16</i>	Nfu_g_1_019328	scaffold01974:4143.21503 (+)	agcatgaaccagcacaacag	tgtggacatcgctctctcaa
<i>wnt4a</i>	Nfu_g_1_003058	scaffold01105:15197.29490 (-)	gcagcagtggaactgga	ggaagccctctggactgact
<i>wnt4b</i>	Nfu_g_1_001049	sgr05:61331906.61335217 (+)	tggcagagtgatgaaccaag	ctgctgaggacagagcatga
<i>wnt5b</i>	Nfu_g_1_011826	sgr01:78418306.78428346 (-)	ccctatgaacctgcacaat	cgcatgacacttacaggaa
<i>tnfrsf11a</i>	Nfu_g_1_011298	sgr08:48409679.48423863 (-)	tgggggtcttaatgagcagt	gagcattgctggcttaac
<i>tnfrsf11b</i>	Nfu_g_1_001796	sgr05:30285084.30304712 (+)	ctcagctgtgcccgtactga	ccagaggcactgaggacag

(Continued on next page)

Continued

Gene Name	Gene Identifier	Position	Forward Primer	Reverse Primer
sox9a	Nfu_g_1_022861	sgr12:41538583.41542084 (-)	taccgcacctccacaac	cgcttctctcttcggtcag
sox9b	Nfu_g_1_019381	sgr03:60962737.60964769 (-)	gcacaacgcagagctcagta	ctacgaacggacgcttctct
runx2	Nfu_g_1_012427	sgr04:67059410.67117221 (-)	ttcaatgatcttcgctttgtg	tgattgtcagcgtgaagctc
sox6	Nfu_g_1_003871	sgr07:16715090.16871623 (+)	ctgtggcctcaacaactg	gctgatgtccaagggtgtca
sp7	Nfu_g_1_021054	sgr10:31084940.31089121 (-)	agggaatgtaattgtaaacacacg	cgaattgttgacggtagca
spp1	Nfu_g_1_018428	sgr02:75958642.75964429 (-)	gggatcagacgagagctcag	tacccagcagctttgaact

QUANTIFICATION AND STATISTICAL ANALYSIS

The data were analyzed by one-way ANOVA with Tukey posttest and expressed as mean \pm standard deviation (SD). $p < 0.05$ was considered statistically significant. All statistical tests were performed using GraphPad PRISM software version 8.0 (GraphPad Software, USA).